HHS Public Access

Author manuscript

J Am Chem Soc. Author manuscript; available in PMC 2019 June 27.

Published in final edited form as:

J Am Chem Soc. 2018 June 27; 140(25): 7764–7768. doi:10.1021/jacs.8b01989.

Single synaptic observation of cholinergic neurotransmission on living neurons: concentration and dynamics

Mei Shen[*], **Zizheng Qu**, **Justin DesLaurier**, **Theresa M. Welle**, **Jonathan V. Sweedler**, and **Ran Chen**

Department of Chemistry, University of Illinois at Urbana-Champaign, 600 South Matthews Avenue, Urbana, IL 61801, USA

Abstract

Acetylcholine, the first neurotransmitter identified more than a century ago, plays critical roles in human activities and health; however, its synaptic concentration dynamics have remained unknown. Here, we demonstrate the *in situ* simultaneous measurements of synaptic cholinergic transmitter concentration and release dynamics. We used nanoscale electroanalytical methods: nanoITIES electrode of 15 nm in radius and nano-resolved scanning electrochemical microscopy (SECM). Time-resolved *in situ* measurements unveiled information on synaptic acetylcholine concentration and release dynamics of living *Aplysia* neurons. The measuring technique enabled the quantitative sensing of acetylcholine with negligible interference of other ionic and redox-active species. We measured cholinergic transmitter concentrations very close to the synapse, with values as high as 2.4 mM. We observed diverse synaptic transmitter concentration dynamics consisting of singlet, doublet and multiplet events with a signal to noise ratio of 6 to 130. The unprecedented details about synaptic neurotransmission unveiled are instrumental for understanding brain communication and diseases in a way distinctive from extra-synaptic studies.

Chemical sensing with electrodes offers chemical identity, quantification, and spatiotemporal information about biological processes in vivo. These advantages make electroanalytical chemistry one of the most widely used tools in the detection of signaling molecules and redox neurotransmitters[1–, 2, 3, 4, 5, 6, 7, 8, 9, 10, 11, 12, 13, 14, 15, 16, 17, 18, 19]. Acetylcholine, the first neurotransmitter identified in 1914 [20, 21] plays a key role in learning, memory and human health; defects in its release have been associated with aging and neurodegeneration. Elucidating its release concentration dynamics at the source of its release, the synaptic cleft, is instrumental in understanding neurodegenerative diseases.

[*]**Corresponding Author:** To whom correspondence should be addressed. mshen233@illinois.edu.

Supporting Information

Experimental section; supplementary text on selectivity of nanoITIES electrodes towards acetylcholine detection; pulling parameters for the nanoITIES and stimulating pipets; voltammograms of ACh detection in ASW background solution with varying concentrations and calibration curve; experimental setup for positive control experiments to confirm the selectivity of nanoITIES electrodes towards ACh detection; results of selectivity of nanoITIES electrodes towards ACh against GABA, glutamate, dopamine, serotonin, high concentration K^+, H^+; amino acid sequence of Pedal peptide; cyclic voltammograms to demonstrate the selectivity of acetylcholine; control experiments to demonstrate that the ACh release was located at single synapse; more experimental results of observed singlet, doublet and multiplet release events for synaptic cholinergic neurotransmission and their occurrence frequency; half peak widths of singlet, doublet and multiplet neurotransmission events; results of SECM approach curve; results of line scan after the SECM approach curve.

The authors declare no competing financial interests.

However, this has been challenging due to the nanometer size of the cleft, with a typical width of 300 nm and a gap of < 100 nm (Fig. 1)[22–, 23, 24, 25, 26, 27] and technical limitation in available nanoprobes for the simultaneous detection of its concentration and release dynamics since acetylcholine is a redox inactive molecule; although carbon nanofiber electrodes have been reported, their detection mainly targets dopamine and norepinephrine, where significant progress has been made[13, 28, 29].

Here we measured in situ simultaneously synaptic acetylcholine concentration and release dynamics with a nanoelectrode of ~15 nm in radius (Fig. 1G). The neuronal model used in the present study is *Aplysia californica*, previously used by Kandel et al. to understand the synapse-specific long-term facilitation[30, 31]; studied pedal ganglion neurons are cholinergic[32, 33, 34] and they were cultured following the well-established protocols [35, 36], with details shown in the Supporting Information. We employed nanoresolved scanning electrochemical microscopy (SECM)[37, 38, 39, 40, 41, 42] (Fig. 1E) to position the nanoelectrode near the synaptic cleft, formed between the axon of one neuron (pink) and the neurite of another neuron (blue) (Figs. 1B, 1F). We detected acetylcholine, based on the charge transfer across a nano interface between two immiscible electrolyte solutions (ITIES), at the nanoITIES pipet electrode [6, 10, 35, 43, 44]. Fig. 1D shows the cyclic voltammogram of acetylcholine detection on the nanoITIES pipet electrode, with calibration curve shown in Fig. S1. We measured the current-time trace at the steady state detection potential, selective for cholinergic transmitter detection (E_{ACh}) against other substances that have been identified or suggested to be released from the *Aplysia* neurons and their vesicles, including serotonin, gamma-aminobutyric acid, dopamine, glutamate *etc.*, as well as the pH change accompanying exocytosis and high concentration K^+ in the stimulating solution, (Control experiments on selectivity shown in Figs. S2-S5, discussion detailed in the supplementary text of the supporting information), to learn about its synaptic release dynamics and concentration profiles.

The results of synaptic cholinergic neurotransmission are shown in Fig. 2 (More results are shown in Figs. S6 and S7). We measured the synaptic release from *Aplysia* neurons in response to high concentration K^+ stimulation and recorded intense release peaks, which are raw data without data processing. Control experiments (Fig. S6) confirm that the measured release appear to be from a single synapse near where the nanoelectrode was located, using a lab-built side view optical microscope and nano-resolution SECM with procedures described under methods section. The detection has high sensitivity as evidenced by a signal to noise ratio from 6 to 130. Direct measurements around the cleft avoid the dilution of transmitter due to its diffusion into the extracellular medium[45, 46, 47], easing the required performance specifications of the small-volume electrochemical measurement. We measured the acetylcholine concentration around the synapse to be as high as 2.4 mM (Figs. 2–3). This measured mM regime of near-synaptic acetylcholine concentration is the same order of magnitude as the number estimated from multiple neuromuscular junctions using stimulated Raman scattering in a recent study[48], and is consistent with the number estimated based on hypothesis and theoretical simulation[49, 50].

The synaptic concentration of neurotransmitter dynamically changes, governed by the combination of multiple processes including its release from presynaptic vesicles, its

reuptake by membrane proteins, its breakdown by the enzymatic reactions, and its diffusion out of the cleft into the extracellular space. The neurotransmitter concentration profiles (Figs. 2A-C, figs. S7A-C) represent this dynamic process. We measured synaptic transmitter concentration dynamic profiles to be composed of singlet, doublet and multiplet (Fig. 2D), with 50% occurrence frequency for singlet and a lower occurrence frequency for doublet and multiplet (Fig. S7D). Our observed occurring frequency of the diverse dynamics for synaptic acetylcholine release is consistent with that of synaptic norepinephrine release measured with carbon nanofiber electrode[29]. More examples of singlet, doublet and multiplet are shown in Fig. S7. For singlet type peaks, the concentration corresponding to neurotransmitter release increases to reach the maxima and then decreases to the base value. In contrast, for doublet and multiplet events, the current did not decrease to the base value after the first peak, and instead it increased to generate the second or even more peaks.

We did quantitative analysis to understand the variation in synaptic transmitter release dynamics. Single vesicular dopamine release studied via carbon electrodes demonstrated half amperometric peak width of hundreds ms, increasing with vesicle sizes[51]. For acetylcholine, the singlet events have half amperometric peak widths of hundreds ms, with multiple values (Fig. S8). This suggests that the singlets be the synaptic single vesicular events, which was further supported by the analysis described in the next paragraph. The variation in half-peak widths are likely due to a distribution of vesicle sizes of Aplysia[52]. Half amperometric peak widths for the doublets totaled two half peak widths of singlets, and that for the multiplets totaled the peak width of multiple singlets (Fig. S8); this applies to all the doublets and multiplets that we observed.

The average number of acetylcholine molecules was 1.0×10^6 for singlet events, and 2.0×10^6 for doublet events (Table. 3B). These quantities are consistent with the amount of acetylcholine needed to produce an end plate potential when acetylcholine was perfused to the neuron muscular junction electrophoretically[53]. Doublets have twice the molecules of the singlets on average (Table 3B). This observation, along with amperometric peak widths discussed above, suggests that doublet and multiplet peaks represent simultaneous release from two or more vesicles (Fig. 2D). Besides, the lower range of the total number of the molecules for doublets and multiplets are similar orders of magnitude to that of the singlets (Table 3B); this suggests the partial release occurrence (Fig. 2E), as proposed in recent studies[54–, 55, 56, 57, 58, 59, 60, 61, 62, 63, 64, 65, 66, 67] during the first peak or the first couple peaks for some of the doublets and multiplets, respectively.

In summary, we have successfully measured cholinergic transmitter release concentration dynamics at the single living *Aplysia* synapse. The work presented here is the first study of the intra-synaptic electrochemical detection of non-redox active transmitter. Our observed diverse release dynamics (singlet, doublet and multiplet) and its occurrence frequency for synaptic acetylcholine release concurred well with that of synaptic norepinephrine release reported in a recent study[29]. Quantitative analysis of half amperometric peak width and of the number of molecules released suggests doublet and multiplet be observation of multiple vesicular events; partial release was suggested as well. Measuring the intra-synaptic dynamics of neurotransmitter release is a critical step in our ability to understand transmission and its deficiencies that are explicated in aging and neurodegenerative diseases.

The new information on the diversity in cholinergic transmitter dynamics and synaptic concentration uncovered will be very valuable for fundamental and biomedical sciences, contributing to our understanding of brain communication and various diseases from a distinctive perspective. Future work includes studying the synaptic release heterogeneity from different kinds of synapses and neuronal types.

Supplementary Material

Refer to Web version on PubMed Central for supplementary material.

ACKNOWLEDGMENT

This work was supported by the National Institute of Neurological Disorders and Stroke of the National Institutes of Health under award numbers R21NS085665 and DA018310. The content is solely the responsibility of the authors and does not necessarily represent the official views of the National Institutes of Health. M. Shen appreciates the start-up fund support from the University of Illinois. T.M.W. is grateful for the support from Dow Chemistry Scholarship for summer research. Z. Q. and J. D. are grateful for the support from their James Scholar Preble Research Awards. SEM was carried out in the Frederick Seitz Materials Research Laboratory Central Research Facilities, University of Illinois at Urbana-Champaign. The authors thank Xiying Wang for the help in preparing *Aplysia* cell cultures. We thank Rhanor Gillette, Joaquin Rodriguez-Lopez and Stanislav Rubakhin for helpful discussions.

REFERENCES

1. Rogers ML; Boutelle MG Real-time clinical monitoring of biomolecules. Annu. Rev. Anal. Chem, 2013, 6, 427–453.
2. Michael AC; Borland LM Ed., Electrochemical Methods for neuroscience, (CRC Press/Taylor & Francis: Boca Raton, FL, 2007).
3. Li Y; Hu K; Yu Y; Rotenberg SA; Amatore C; Mirkin MV Direct Electrochemical Measurements of Reactive Oxygen and Nitrogen Species in Nontransformed and Metastatic Human Breast Cells. J. Am. Chem. Soc, 2017, 139, 13055–13062. [PubMed: 28845981]
4. Gordito MP; Kotsis DH; Minteer SD; Spence DM Flow-based amperometric detection of dopamine in an immobilized cell reactor. J. Neurosci Methods, 2003, 124, 129–134 [PubMed: 12706842]
5. Amatore C; Arbault S; Guille M; Lemaître F Electrochemical monitoring of single cell secretion: vesicular exocytosis and oxidative stress. Chem. Rev, 2008, 108, 2585–2621. [PubMed: 18620370]
6. Amemiya S; Kim J; Izadyar A; Kabagambe B; Shen M; Ishimatsu R Electrochemical sensing and imaging based on ion transfer at liquid/liquid interfaces. Electrochimica Acta, 2013, 110, 836–845.
7. Garris PA; Kilpatrick M; Bunin MA; Michael D; Walker QD; Wightman RM Dopamine transients are sufficient and necessary for acquisition of model-based associations. Nature, 1999, 398, 67–69. [PubMed: 10078530]
8. Polcari D; Dauphin-Ducharme P; Mauzeroll J Scanning electrochemical microscopy: a comprehensive review of experimental parameters from 1989 to 2015. Chem. Rev, 2016, 116, 13234–13278. [PubMed: 27736057]
9. Zhang B; Heien MLAV; Santillo MF; Mellander L; Ewing AG Temporal Resolution in Electrochemical Imaging on Single PC12 Cells Using Amperometry and Voltammetry at Microelectrode Arrays. Anal. Chem 2011, 83, 571–577. [PubMed: 21190375]
10. Shen M; Colombo ML Electrochemical nanoprobes for the chemical detection of neurotransmitters. Analytical Methods, 2015, 7, 7095–7105. [PubMed: 26327927]
11. Hashemi P; Dankoski EC; Lama R; Wood KM; Takmakov P; Wightman RM Brain dopamine and serotonin differ in regulation and its consequences. Proc. Nat. Ac. Sci. U.S.A, 2012, 109, 11510–11515.
12. Ge S; Koseoglu S; Haynes CL Bioanalytical tools for single-cell study of exocytosis. Anal. Bioanal. Chem, 2010, 397, 3281–3304. [PubMed: 20521141]

13. Amatore C; Arbault S; Bonifas I; Bouret Y; Erard M; Ewing AG; Sombers LA Correlation between vesicle quantal size and fusion pore release in chromaffin cell exocytosis. Biophys. J, 2005, 88, 4411–4420. [PubMed: 15792983]
14. Wang K; Xiao T; Yue Q; Wu F; Yu P; Mao L Selective amperometric recording of endogenous ascorbate secretion from a single rat adrenal chromaffin cell with pretreated carbon fiber microelectrodes. Anal. Chem, 2017, 89, 9502–9507. [PubMed: 28776368]
15. Rees HR; Anderson SE; Privman E; Bau HH; Venton BJ Carbon nanopipette electrodes for dopamine detection in Drosophila. Anal. Chem, 2015, 87, 3849–3855. [PubMed: 25711512]
16. Yin B; Barrionuevo G; Weber SG Optimized real-time monitoring of glutathione redox status in single pyramidal neurons in organotypic hippocampal slices during oxygen-glucose deprivation and reperfusion. ACS Chem. Neurosci, 2015, 6, 1838–1848. [PubMed: 26291433]
17. Andrews A Why Monitor Molecules in Neuroscience? ACS Chem. Neurosci, 2017, 8, 211–212. [PubMed: 28196419]
18. Hu MJ; Fritsch I Redox cycling behavior of individual and binary mixtures of catecholamines at gold microband electrode arrays. Anal. Chem, 2015, 87, 2029–2032. [PubMed: 25609159]
19. Perry M; Li Q; Kennedy RT Review of recent advances in analytical techniques for the determination of neurotransmitters. Anal. Chim. Acta, 2009, 653,1–22. [PubMed: 19800472]
20. Dale HH The action of certain esters and ethers of choline, and their relation to muscarine. J. Pharm. Exp. Ther, 1914, 6, 147–190.
21. Loewi O Über humorale Übertragbarkeit der Herznervenwirkung. Pflügers Arch. Ges. Physiol, 1921, 189, 239–242.
22. McCann ME; Vanherberqhen B; Eleme K; Carlin LM; Newsam RJ; Goulding D; Davis DM The size of the synaptic cleft and distinct distributions of filamentous actin, ezrin, CD43 and CD45 at activating and inhibitory human NK cell immune synapses. J. Immunol, 2003, 170, 2862–2870. [PubMed: 12626536]
23. Brossard C; Feuillet V; Schmitt A; Randriamampita C; Roman M; Raposo G; Trautmann A Multifocal structure of the T cell – dendritic cell synapse. Eur. J. Immunol, 2005, 35, 1741–1753. [PubMed: 15909310]
24. Moukhles H; Bosler O; Bolam JP; Vallee A; Umbriaco D; Geffard M; Doucet G Quantitative and morphometric data indicate precise cellular interactions between serotonin terminals and postsynaptic targets in rat substania nigra. Neuroscience, 1997, 76, 1159–1171. [PubMed: 9027876]
25. Groves PM; Linder JC; Young SJ 5-hydroxydopamine-labeled dopaminergic axns: three-dimensional reconstruction of axons, synapses and postsynaptic targets in rat neostriatum. Neuroscience, 1994, 58, 593–604. [PubMed: 8170539]
26. Pickel VM; Beckley SC; Joh TH; Reis DJ Ultrastructural immunocytochemical localization of tyrosine hydroxylase in the neostriatum. Brain Res, 1981, 225, 373–385. [PubMed: 6118197]
27. Dani A; Huang B; Bergan J; Dulac C; Zhuang X Superresolution imaging of chemical synapses in the brain. Neuron, 2010, 68, 843–856. [PubMed: 21144999]
28. Li YT; Zhang SH; Wang XY; Zhang XW; Oleinick AI; Svir I; Amatore C; Huang WH Real-time monitoring of discrete synaptic release events and excitatory potentials within self-reconstructed neuromuscular junctions. Angew. Chem. Int. Ed, 2015, 54, 9313–9318.
29. Li YT; Zhang SH; Wang L; Xiao RR; Liu W; Zhang XW; Zhou Z; Amatore C; Huang WH Nanoelectrode for ameperometric monitoring of individual vesicular exocytosis inside single synapses. Angew. Chem. Int. Ed, 2014, 53, 12456–12460.
30. Martin KC; Casadio A; Zhu H; Yaping E; Rose JC; Chen M; Bailey CH; Kandel ER Synapse-specific, long-term facilitation of aplysia sensory to motor synapse: a function for local protein synthesis in memory storage. Cell, 1997, 91, 927–938. [PubMed: 9428516]
31. Kandel ER The molecular biology of memory storage: a dialogue between gene and synapses. Science, 2001, 294, 1030–1038. [PubMed: 11691980]
32. McCaman RE; Dewhurst SA Choline acetyltransferase in individual neurons of Aplysia californica. Journal of Neurochemistry, 1970, 17, 1421–1426. [PubMed: 5496391]
33. Eisenstadt M; Goldman JE; Kandel ER; Koike H; Koester J; Schwartz JH Intrasomatic injection of radioactive precursors forstudying transmitter synthesis in identified neurons of Aplysia

californica. Proceedings of the National Academy of Sciences of the United States of America, 1973, 70, 3371–3375. [PubMed: 4519630]

34. Moroz LL; Edward JR; Puthanveettil SV; Kohn AB; Ha T; Heyland A; Knudsen B; Sahni A; Yu F; Liu L; Jezzini S; Lovell P; Iannucculli W; Chen M; Nguyen T; Sheng H; Shaw R; Kalachikov S; Panchin YV; Farmerie W; Russo JJ; Ju J; Kandel ER Neuronal transcriptome of Aplysia: neuronal compartments and circuitry. Cell, 2006, 127, 1453–1467. [PubMed: 17190607]
35. Le A-P; Kang S; Thompson LB; Rubakhin SS; Sweedler JV; Rogers JA; Nuzzo RG Quantitative reflection imaging of fixed Aplysia californica pedal ganglion neurons on nanostructured plasmonic crystals. J. Phys. Chem. B, 2013, 117, 13069–13081. [PubMed: 23647567]
36. Kang S; Badea A; Rubakhin SS; Sweedler JV; Rogers JA; Nuzzo RG Quantitative reflection imaging for the morphology and dynamics of live Aplysia californica pedal ganglion neurons cultured on nanostructured plasmonic crystals. Langmuir, 2017, 33, 8640–8650. [PubMed: 28235182]
37. Chen Q; Luo L; Faraji H; Feldberg SW; White HS Electrochemical measurement of single H_2 nanobubble nucleation and stability at Pt nanoelectrodes. J. Phys. Chem. Lett, 2014, 5, 3539–3544. [PubMed: 26278606]
38. Shen M; Ishimatsu R; Kim J; Amemiya S Quantitative imaging of ion transport through single nanopores by high-resolution scanning electrochemical microscopy. J. Am. Chem. Soc, 2012, 134, 9856–9859. [PubMed: 22655578]
39. Bard AJ; Mirkin MV Ed., Scanning Electrochemical Microscopy (CRC Press/Taylor & Francis: Boca Raton, FL, ed. 2, 2012).
40. Mirkin MV; Sun T; Yu Y; Zhou M Electrochemistry at one nanoparticle. Acc. Chem. Res, 2016, 49, 2328–2335. [PubMed: 27626289]
41. Chen R; Balla RJ; Lima A; Amemiya S Characterization of nanopipet-supported ITIES tips for scanning electrochemical microscopy of single-state nanopores. Anal. Chem, 2017, 89, 7269–7272. [PubMed: 28597652]
42. Amemiya S; Mirkin MV Eds. Nanoelectrochemistry, (Taylor and Francis: Boca Raton, FL, 2015).
43. Amemiya S; Wang Y; Mirkin MV Nanoelectrochemistry at the liquid/liquid interfaces. Electrochemistry. 2014, 12, 1–43.
44. Colombo ML; Sweedler JV; Shen M Nanopipet-based liquid-liquid interface probes for the electrochemical detection of acetylcholine, tryptamine, and serotonin via ionic transfer. Anal. Chem, 2015, 87, 5095–5100. [PubMed: 25877788]
45. Bunin MA; Wightman RM Quantitative evaluation of 5-hydroxytryptamine (serotonin) neuronal release and uptake: an investigation of extrasynaptic transmission. J. Neurosci, 1998, 18, 4854–4860. [PubMed: 9634551]
46. Garris PA; Ciolkowski EL; Pastore P; Wightman RM Efflux of dopamine from the synaptic cleft in the nucleus accumbens of the rat brain. J. Neurosci, 1994, 14, 6084–6093. [PubMed: 7931564]
47. Rice ME; Nicholson C Diffusion characteristics and extracellular volume fraction during normoxia and hypoxia in slices of rat neostriatum. J. Neurophysiol, 1991, 65, 264–272. [PubMed: 2016641]
48. Fu D; Yang W; Xie XS Label-free imaging of neurotransmitter acetylcholine at neuromuscular junctions with stimulated Raman scattering. J. Am. Chem. Soc, 2017, 139, 583–586. [PubMed: 28027644]
49. Matthews-Bellinger J; Salpeter MM Distribution of acetylcholine receptors at frog neuromuscular junctions with a discussion of some physiological implications. J. Physiol, 1978, 279, 197–213. [PubMed: 307600]
50. Scimemi A; Beato M Determing the neurotransmitter concentration profile at active synapses. Mol. Neurobiol, 2009, 40, 289–306. [PubMed: 19844813]
51. Cans AS; Wittenberg N; Karlsson R; Sombers L; Karlsson M; Orwar O; Ewing A Artificial cells: unique insights into exocytosis using liposomes and lipid nanotubes. Proc. Natl. Acad. Sci. U. S. A, 2003, 100, 400–404. [PubMed: 12514323]
52. Gillete R; Pomeranz B Ultrastructural correlates of interneuronal function in the abdominal ganlion of Aplysia californica. J. Neurobiol, 1975, 6, 463–474. [PubMed: 1176980]
53. Krnjević K; Miledi R Acetylcholine in mammalian neuromuscular transmission. Nature, 1958, 182, 805–806.

54. Omiatek DM; Dong Y; Heien ML; Ewing AG Only a fraction of quantal content is released during exocytosis as revealed by electrochemical cytometry of secretory vesicles. ACS Chem. Neurosci, 2010, 1, 234–245. [PubMed: 20368748]
55. Wightman RM; Haynes CL Synaptic vesicles really do kiss and run. Nat. Neurosci, 2004, 7, 321–322. [PubMed: 15048116]
56. Ren L; Mellander LJ; Keighron J; Cans A-S; Kurczy ME; Svir I; Oleinick A; Amatore C; Ewing AG The evidence for open and closed exocytosis as the primary release mechanism. Q. Rev. Biophys, 2016, 49, e12. [PubMed: 27659043]
57. Amatore C; Arbault S; Bonifas I; Bouret Y; Erard M; Ewing AG; Sombers LA Correlation between vesicle quantal size and fusion pore release in chromaffin cell exocytosis. Biophys. J, 2005, 88, 4411–4420. [PubMed: 15792983]
58. Amatore C; Arbault S; Bouret Y; Guille M; Lemaitre F; Verchier Y Regulation of exocytosis in chromaffin cells by trans-insertion of lysophosphatidylcholine and arachidonic acid into the outer leaflet of the cell membrane. ChemBioChem, 2006, 7, 1998–2003. [PubMed: 17086558]
59. Amatore C; Arbault S; Bonifas I; Guille M; Lemaitre F; Verchier Y Relationship between amperometric pre-spike feet and secretion granule composition in chromaffin cells: an overview. Biophys. Chem, 2007, 129, 181–189. [PubMed: 17587484]
60. Amatore C; Arbault S; Bonifas I; Guille M Quantitative investigations of amperometric spike feet suggest different controlling factors of the fusion pore in exocytosis at chromaffin cells. Biophys. Chem, 2007, 143, 124–131.
61. Amatore C; Oleinick AI; SVIR I Reconstruction of aperture functions during full fusion in vesicular exocytosis of neurotransmitters. ChemPhysChem, 2010, 11, 159–174. [PubMed: 19937905]
62. Omiateck DM; Dong Y; Heien ML; Ewing AG Only a fraction of quantal content is released during exocytosis as revealed by electrochemical cytometry of secretory vesicles. ACS Chem. Neurosci, 2010, 1, 234–245. [PubMed: 20368748]
63. Keighron JD; Ewing AG; Cans A-S Analytical tools to monitor exocytosis: a focus on new fluorescent probes and methods. Analyst, 2012, 137, 1755–1763. [PubMed: 22343677]
64. Mellander LJ; Kurczy ME; Najafinobar N; Dunevall N; Ewing AG; Cans A-S Two modes of exocytosis in an artificial cell. Sci. Rep, 2014, 4, 3847. [PubMed: 24457949]
65. Phan NT; Li X; Ewing AG Measuring synaptic vesicles using cellular electrochemistry and nanoscale molecular imaging. Nature Rev, 2017, 1, 0048.
66. Dunevall J; Majdi S; Larsson A; Ewing A Vesicle impact electrochemical cytometry compared to amperometric exocytosis measurements. Curr. Opin. Electrochem, 2017, 5, 85–91. [PubMed: 29218327]
67. Li X; Dunvall J; Ewing AG Quantitative chemical measurements of vesicular transmitters with electrochemical cytometry. Acc. Chem. Res, 2016, 49, 2347–2354. [PubMed: 27622924]

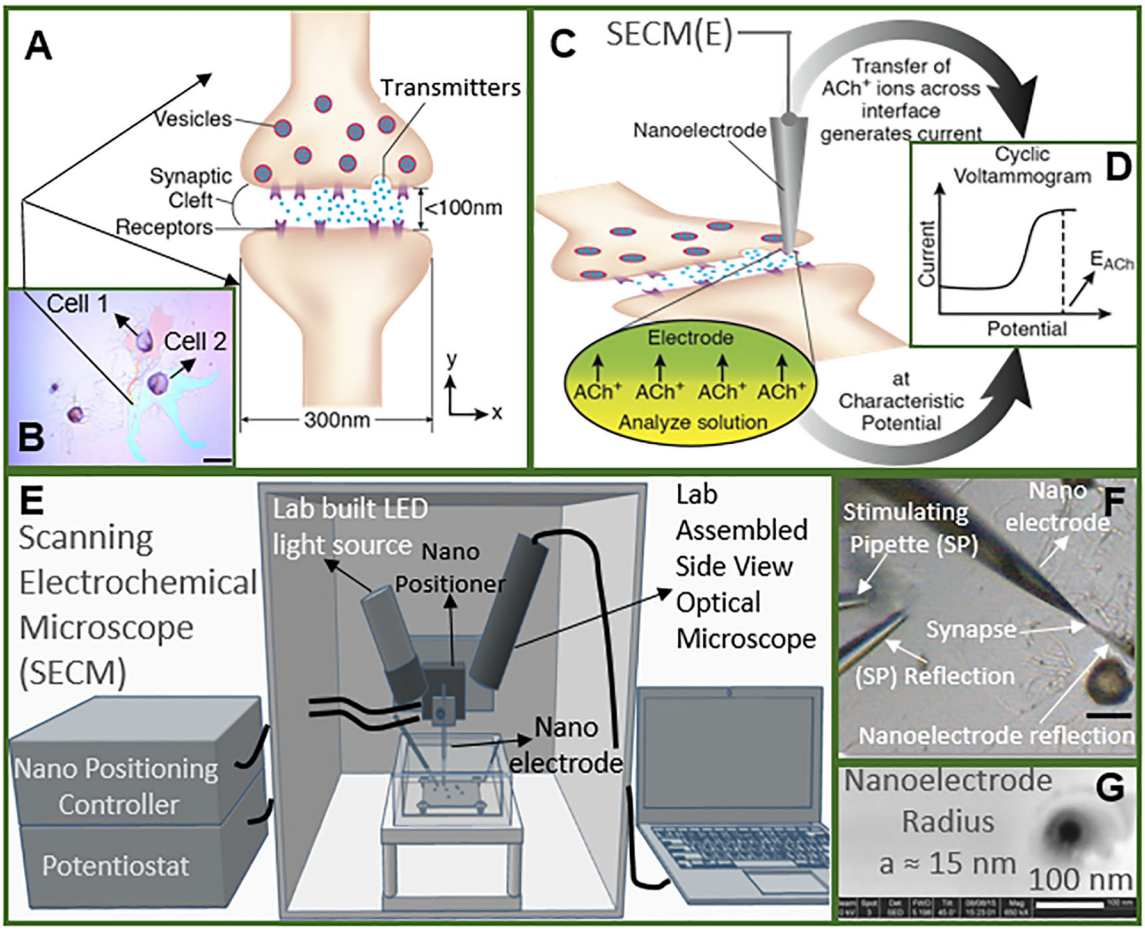

Figure 1.

Study of cholinergic neurotransmission at single synaptic cleft with nanoelectrode and scanning electrochemical microscope. (A) Illustration of synaptic cleft dimensions[22–, 23, 24, 25, 26, 27]. (B) Cultured living Aplysia pedal ganglion neurons used for the experiment, where the axon from cell 1 (pink) formed a synaptic connection with the body of cell 2. Scale bar: 200 μm. (C) A nanoITIES pipet electrode was positioned around the synaptic cleft to measure the concentration and release dynamics of acetylcholine (ACh^+) simultaneously using amperometry; the positioning of the nanoelectrode was achieved using the scanning electrochemical microscope (Fig. E) with a spatial resolution of 5 nm. The zoom shows the nanoITIES formed at the tip of the nanoITIES pipet electrode, and ionic transmitter (ACh^+) transfers across the interface, generating a current and thus getting detected. (D) Cyclic voltammogram corresponding to ACh detection, where the detection potential follows Nernstian equation, and a steady state transfer potential, E_{ACh}= - 0.48 V vs $E_{1/2,\ TBA}$, selective for cholinergic neurotransmitter detection was used in amperometry to study its synaptic concentration dynamics (results shown in Figs. 2 and 3). (E) A Scanning Electrochemical Microscope (SECM) and a lab-built side view optical microscope were used for the positioning of the nanoelectrode around synapses with nm spatial resolution. The lab-built side view optical microscope provided rough positioning before the fine positioning of 5 nm spatial resolution with SECM. After SECM positioning (Supporting

Information, figs. S9, S10), the optical microscopic view of the nanoelectrode and the synapse are shown in Fig. F, where it can be seen that it is very hard to locate the synapse by visual observation alone. The combined use of the side view optical microscope and nano-positioning platform, SECM, is critical. (F) A stimulating pipet was used to provide high concentration K^+ stimulation. Reflection was used for the rough positioning of the nanoelectrode and stimulating pipet in the x, y and z axes by optical microscope, which was followed by the nanometer positioning of the nanoelectrode around the synapse achieved using nano-resolution SECM with details described in the supporting information. Scale bar: 150 μm. (G) High resolution scanning electron microscope (SEM) picture of the nanopipet tip with radius (a) to be around 15 nm.

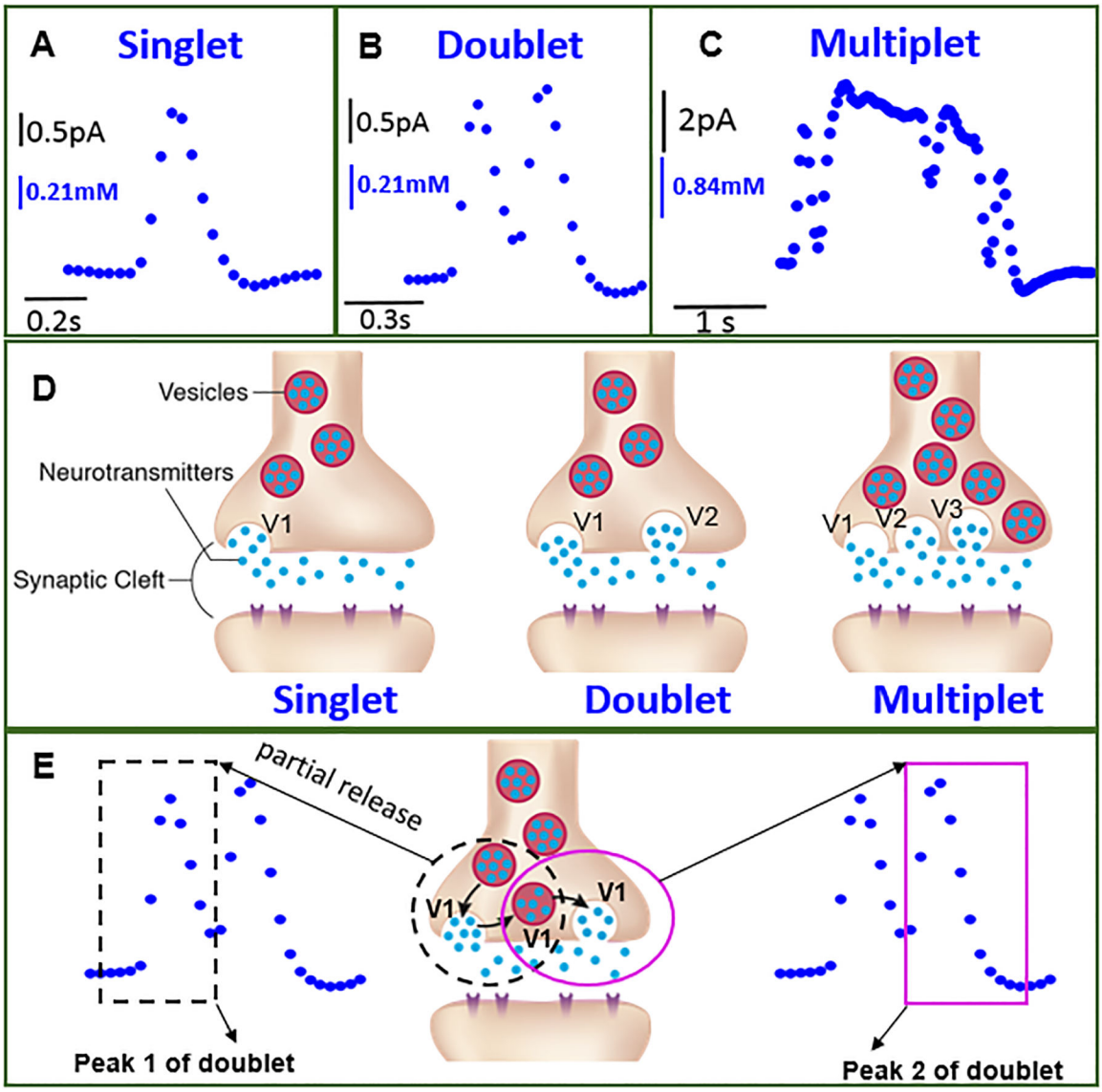

Figure 2.

Single synaptic cholinergic neurotransmission measured *in situ*. (**A**-**C**) Current-time trace (amperometry) representing synaptic transmitter concentration and release dynamics simultaneously, where diverse cholinergic concentration dynamics were observed consisted of singlet (Fig. **A**), doublet (Fig. **B**), and multiplet (Fig. **C**). Single current (concentration) maxima occur during singlet release (50% occurrence frequency out of 16 events total); a second current maximum occurs before the first current peak decreases to the base value for the doublet events (~30% occurrence frequency); multiple concentration peaks (more than two) were observed for multiplet with lower occurrence frequency (~20%) (Fig. S7D). (**D**) Proposed mechanism on variation in synaptic transmitter release dynamics. Neurotransmitter is released into the synaptic cleft from a single vesicle (Left). Neurotransmitter is released into the synaptic cleft from two vesicles, V1 and V2, simultaneously (Middle) or multiple vesicles simultaneously, which are going through either different stages of exocytosis as shown here, or similar stages of exocytosis (Right). (**E**) An alternative mechanism is

possible for explaining doublets and multiplets based on the phenomenon of partial release[54–67]. A vesicle goes through partial release twice, generating a doublet (Middle); the two individual peaks (Peak 1 and Peak 2) correspond to each partial release event.

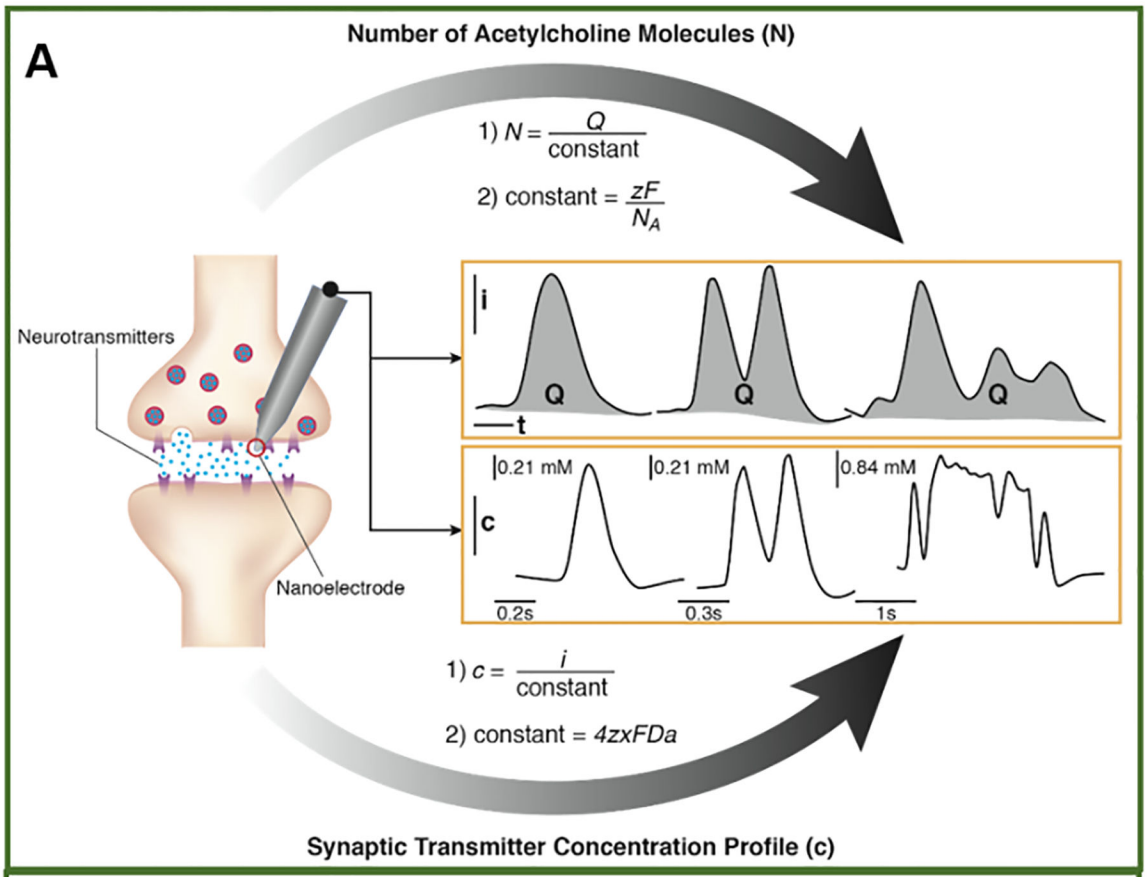

B

Synaptic Concentration Dynamics	Number of Molecules (Range)	Number of Molecules (Median)	Number of Moles (mmol) (Range)	Number of Moles (mmol) (Median)
Singlet	$4.3x10^5$- $2.6x10^6$	$1.0x10^6$	$7.1x10^{-16}$- $4.2\ x10^{-15}$	$1.7\ x10^{-15}$
Doublet	$6.5x10^5$ – $4.3x10^6$	$2.0x10^6$	$1.1x10^{-15}$- $7.2\ x10^{-15}$	$3.4\ x10^{-15}$
Multiplet	$1.4x10^6$ - $6.3x10^7$	$2.0x10^7$	$2.4x10^{-15}$- $1.1\ x10^{-13}$	$3.3\ x10^{-14}$

Figure 3.

Simultaneous determination of the synaptic cholinergic transmitter concentration dynamics and the number of transmitter molecules (N) during discrete synaptic release events (**A**). N_A is Avogadro's number, Q is the charge based on integration of amperometric current peak, z is the charge of the transmitter molecule (equals 1 for acetylcholine), and F is Faraday's constant. Synaptic transmitter concentration profile was obtained from amperometric peak based on current expression at the nanoelectrode, $c = \frac{i}{4xzFDa}$ (Supporting Information). (**B**) Number of neurotransmitter molecules and number of moles released during singlet (N = 8), doublet (N = 4) and multiplet events (N = 4) measured from the single synapse shown in Fig. 1B in response to 6 repetitive chemical stimulations. Release events were constantly observed during each of six chemical stimulations. A variation in synaptic cholinergic

transmitter concentration was observed, which is likely due to variation in synaptic vesicles sizes as observed by TEM[52].